Probability mapping of soil thickness by random survival forest at a national scale

Songchao Chen, Vera Leatitia Mulder, Manuel M. Martin, Christian Walter, Marine Lacoste, Anne C Richer-De-Forges, Nicolas P.A. Saby, Thomas Loiseau, Bifeng Hu, Dominique Arrouays

Title: Probability mapping of soil thickness by random survival forest at a national scale

Authors:

Songchao Chen [a, b]. songchao.chen@inra.fr

Vera Leatitia Mulder [c]. titia.mulder@wur.nl

Manuel P. Martin [a]. manuel.martin@inra.fr

Christian Walter [b]. christian.walter@agrocampus-ouest.fr

Marine Lacoste [d]. marine.lacoste@inra.fr

Anne C. Richer-de-Forges [a]. anne.richer-de-forges@inra.fr

Nicolas P.A. Saby [a]. nicolas.saby@inra.fr

Thomas Loiseau [a]. thomas.loiseau@inra.fr

Bifeng Hu [a, d, e]. bifeng.hu@inra.fr

Dominique Arrouays [a]. dominique.arrouays@inra.fr

Affiliations:

[a] INRA, Unité InfoSol, 45075 Orléans, France

[b] SAS, INRA, Agrocampus Ouest, 35042 Rennes, France

[c] Soil Geography and Landscape group, Wageningen University, PO Box 47 6700 AA Wageningen, The Netherlands

[d] INRA, Unité Science du sol, 45075 Orléans, France

[e] Sciences de la Terre et de l'Univers, Orléans University, 45067 Orléans, France

Corresponding author:

Songchao Chen: songchao.chen@inra.fr

Postal address: INRA, Unité InfoSol, 2163 Avenue de la Pomme de Pin, CS 40001 Ardon, 45075 Orléans, France

Telephone: +33(0)602142667

Abstract:

Soil thickness (ST) is a crucial factor in earth surface modelling and soil storage capacity calculations (e.g., available water capacity and carbon stocks). However, the observed depths recorded in soil information systems for some profiles are often less than the actual ST (i.e., right censored data). The use of such data will negatively affect model and map accuracy, yet few studies have been done to resolve this issue or propose methods to correct for right censored data. Therefore, this work demonstrates how right censored data can be accounted for in the ST modelling of mainland France. We propose the use of Random Survival Forest (RSF) for ST probability mapping within a Digital Soil Mapping framework. Among 2109 sites of the French Soil Monitoring Network, 1089 observed STs were defined as being right censored. Using RSF, the probability of exceeding a given depth was modelled using freely available spatial data representing the main soil-forming factors. Subsequently, the models were extrapolated to the full spatial extent of mainland France. As examples, we produced maps showing the probability of exceeding the thickness of each *GlobalSoilMap* standard depth: 5, 15, 30, 60, 100, and 200 cm. In addition, a bootstrapping approach was used to assess the 90% confidence intervals. Our results showed that RSF was able to correct for right censored data entries occurring within a given dataset. RSF was more reliable for thin (0.3 m) and thick soils (1 to 2 m), as they performed better (overall accuracy from 0.793 to 0.989) than soils with a thickness between 0.3 and 1 m. This study provides a new approach for modelling right censored soil information. Moreover, RSF can produce probability maps at any depth less than the maximum depth of the calibration data, which is of great value for designing additional sampling campaigns and decision making in geotechnical engineering.

Keywords: Soil thickness modelling; Right censored data; Random Survival Forest; GlobalSoilMap; Probability mapping.

1. Introduction

Soils are of great importance in supporting, provisioning, and regulating ecosystem services, such as food production and climate change mitigation (Clothier et al., 2011; Keesstra et al., 2016; Millennium Ecosystems Assessment, 2005). As stated by recent studies (e.g., Bouma, 2018; Groshans et al., 2018; Marx et al., 2019), there is a rising demand for up-to-date and ecosystem service relevant soil information. Therefore, substantial effort is needed to communicate soil information among diverse audiences and produce fine resolution soil maps to support practical land management. In this study, we use the *GlobalSoilMap* project specifications. These specifications focus on delivering consistently produced high-resolution soil property information throughout the world by predicting mean values and their prediction intervals (PIs) (Arrouays et al., 2014a; Arrouays et al., 2014b; Sanchez et al., 2009). Among the twelve soil properties to be predicted following the recommendations of *GlobalSoilMap*, soil thickness (ST) is a key property. In this study, in line with *GlobalSoilMap*, ST is defined as 'the depth (cm) from the soil surface to the lithic or a paralithic contact' (Soil Survey Division Staff, 1993). The ST is highly relevant for soil hydro-mechanical modelling (Tesfa et al., 2009; Wang et al., 2006), soil erosion impact, landscape evolution, vegetation growth (Heimsath et al., 2001; Meyer et al., 2007), and for calculating soil functions (e.g., available water capacity (Leenaars et al., 2018; Román Dobarco et al., 2019), soil structure (Rabot et al., 2018; Vogel et al., 2018), and soil organic carbon stocks (Batjes, 1996; Chen et al., 2019)). Despite the great importance of accurate ST information, the large spatial variability and high cost of ST measurements make ST determination difficult (Lacoste et al., 2016). Discordance in the definition of ST also hampers ST modelling, especially when data are collected from various projects (Lacoste et al., 2016). The

observed ST recorded in soil information systems for some profiles are often less than the actual ST (i.e., right censored data).

ST results from the mass balance between soil formation from the bedrock and soil transport by erosion and sedimentation (Heimsath et al., 1997; Heimsath et al.,1999); thus, it varies as a function of physical, chemical, and biological processes (Román et al., 2018). ST can be related to these processes by modeling the relationship between the main soil-forming factors, i.e., Jenny's Soil-Landscape paradigm (Jenny,1941): parent material, climatic conditions, organisms, terrain relief, and time (Dietrich et al., 1995; Minasny and McBratney, 1999). More recently, McBratney et al. (2003) formulated the concept of the SCORPAN model, which also includes also soil information and spatial location.

Various approaches for ST modelling and mapping have relied on modelling the relationship between the main soil forming factors. The majority of these approaches can be broadly classified into two groups: 1) physically based and mechanistic models, which predict ST using soil process models based on the rates of weathering, denudation, and accumulation (Bonfatti et al., 2018; Dietrich et al., 1995; Minasny and McBratney, 1999; Pelletier and Rasmussen, 2009); and 2) empirical models, including statistical and geostatistical methods (Kuriakose et al., 2009). These models rely on the empirical relationships between ST and explanatory covariates of inferential attributes (e.g., plant species, precipitation, and parent material).

For the latter, a wide range of statistical methods have been previously applied in ST modelling, including canonical correspondence analysis and principal component analysis (Odeh et al., 1991), multiple linear regression (Moore et al., 1993), expert knowledge and fuzzy logic (Zhu et al., 2001), Generalized Additive

104 Models and Random Forest (Tesfa et al., 2009), and Cubist and Gradient Boosting
105 Modelling (Lacoste et al., 2016; Mulder et al., 2016a).
106 Within the field of geostatistics, various kriging techniques have often been
107 used to predict and spatially interpolate ST from point samples. Ordinary Kriging was
108 most commonly used among these kriging techniques (Penížek and Borůvka, 2006;
109 Vanwalleghem et al., 2010). The prediction variance was typically reduced when
110 including additional prediction variables using regression kriging (Kuriakose et al.,
111 2009; Odeh et al., 1995) or Kriging with External Drift (Bourennane et al., 1996;
112 Kempen et al., 2015).
113 None of the studies referred to above addressed the issue of having right
114 censored data entries in their soil databases. However, it is often the case that the
115 actual ST is thicker than the observed ST, which can mainly be attributed to practical
116 constraints, such as the standard auger length (120 cm), and time constraints. In fact,
117 in soil sciences very few studies consider the effect of right censored data; the issue
118 is often ignored or processed by adding a fixed value (e.g., 30 cm) in ST modelling
119 (Knotters et al., 1995; Vaysse and Lagacherie, 2015; Lacoste et al., 2016;
120 Shangguan et al., 2017). Some previous works dealt with left censored data,
121 especially regarding data below detection limits (e.g., de Oliveira, 2005; Fridley and
122 Dixon, 2007; Orton et al., 2009; Orton et al., 2012; Villaneau et al., 2011). Ignoring
123 the presence of right censored data entries within a database and relying on the
124 observed ST for those entries will result in an underestimation of modelled ST
125 (Vaysse and Lagacherie, 2015; Shangguan et al., 2017).
126 However, right censored data are commonly used in statistics and medical
127 research, especially in survival analysis. Several models have been used to deal with
128 right censored data in survival analysis, including the Kaplan Meier method (Kaplan

and Meier, 1958), Cox regression (Andersen and Gill, 1982), and Random Survival Forest (RSF, Ishwaran et al., 2008). The Kaplan Meier method and Cox regression mainly deal with linear effects, but RSF is capable of handling complex non-linear effects that may exist between predictor variables (Mogensen et al., 2012). Therefore, as previously suggested by Styc and Lagacherie (2016), RSF may have the best potential for identifying and correcting right censored data used for Digital Soil Mapping (DSM).

In this study, the potential of RSF was evaluated for ST mapping in mainland France. The main objectives of this study are noted below:

1) Apply RSF for mapping the probability of exceeding a certain ST using both actual and right censored ST data from the French Soil Monitoring Network (RMQS) and
2) Derive the 90% confidence intervals of the specific ST using bootstrapping.

2. Material and methods

2.1. Soil dataset

We used ST data from the RMQS soil database that were gathered between 2001 and 2009 (Jolivet et al., 2006), covering different soil, climate, relief, and land cover conditions (Fig. 1). The RMQS dataset is based on a 16 km × 16 km square grid where all sites are selected at the centre of each grid cell. When sampling the exact location was not possible, a site was selected as close as possible to the grid centre. A soil pit was dug, and the surrounding information (land use and geomorphology) and a detailed description of the soil profile were recorded for each site, including soil horizon depth and ST. Auger boring was recommended (but not mandatory) to complete the soil profile when the soil pit was not thick enough to

154 determine the ST. For more detailed information about the soil sampling design and
155 laboratory analysis, see Chen et al. (2018). Among 2109 RMQS sites, ST was
156 explicitly recorded for 1020 sites (down to a lithic or paralithic contact), while the
157 remaining 1089 sites were right censored data. The ST for nine RMQS sites was set
158 to 0, as these sites were identified as mountainous sites with bare rock.
159
160 2.2. Exhaustive covariates
161 We used a DSM framework (McBratney et al., 2003) to model the relationships
162 between ST and ancillary covariates (Table 1). These covariates cover a series of
163 soil formation related environmental factors, including soil, climate, organisms, relief
164 and parent material. Before modelling, these covariates were re-projected to Lambert
165 93 (official projection for mainland France) and resampled to a 90 m resolution (in
166 raster format) using a bilinear interpolation (numeric covariates) or nearest neighbour
167 (categorical covariates).
168
169 2.3. Random survival forest for probability modelling of soil thickness
170 2.3.1. General introduction
171 RSF is an ensemble tree method for modelling right censored survival data
172 (Ishwaran et al., 2008). RSF is an extension of Breiman's (2001) random forest (RF),
173 known as an ensemble learning approach that is improved by injecting randomization
174 into the base-learning process. For example, using a human analogy, a specific
175 status introduced in RSF aims to distinguish whether it is a death case (status = 1) or
176 a survival case (status = 0) at a given observed time. The RSF does this by
177 estimating the presence-absence probability. Applying this censoring concept to ST,
178 at a given site there are two possibilities for a thickness to be recorded: i) the actual

ST has been observed down to lithic or paralithic contact as defined before (status = 1) or ii) the lithic or paralithic contact has not been reached and the actual ST remains unknown (status = 0). For the latter, it is only known that the actual ST is greater than the observed ST. RSF uses a new type of predicted outcome that contains a cumulative hazard function (CHF, see Section 2.3.2).

2.3.2. Random survival forest model fitting

RSF model fitting involves the following steps (Ishwaran et al., 2008), as shown in Fig. 2.

1) Select *ntree* bootstrapped samples from the calibration data. Approximately 37% (e^{-1}) of the calibration data are excluded in each bootstrapped sample, which are so-called out-of-bag (OOB) data.
2) Grow a survival tree for each bootstrapped sample. At each node of the survival tree, randomly select *mtry* covariates for splitting the data. Survival splitting criteria are then used, and each node is split on that covariate, which maximizes survival differences across sub-nodes.
3) Grow the survival tree to full size under the constraint that a terminal node should have no less than *nodesize* unique actual ST samples.
4) Calculate a CHF for each survival tree and obtain the ensemble CHF by averaging all the survival trees for each sample.
5) Calculate the prediction error of the ensemble CHF based on OOB data.

Ensemble cumulative hazard function and ensemble survival function

Constructing the ensemble CHF is crucial for RSF. Hereafter, we provide details about the procedure for a better understanding.

For a survival tree, let ($ST_{1,h}$, $\delta_{1,h}$), . . . ,($ST_{n(h),h}$, $\delta_{n(h),h}$) be the observed ST and the 0–1 censoring status (δ) for n samples in a terminal node h. Here, let $ST_{1,h} < ST_{2,h} < \cdots < ST_{n(h),h}$ be the different observed ST in the terminal node. The CHF estimate for h is then defined by the Nelson–Aalen estimator $\widehat{H}_h$:

$$\widehat{H}_h(st) = \sum_{st_{l,h} \le st} \frac{a_{l,h}}{Y_{l,h}}, \quad (1)$$

where $a_{l,h}$ and $Y_{l,h}$ are the number of actual ST samples and all samples at observed ST $st_{l,h}$, respectively. All the samples within the terminal node h have the same CHF.

Each sample i has a *mtry*-dimensional covariate $\mathbf{x}_i$ that will belong to a unique terminal node h. Therefore, the CHF for i is the Nelson–Aalen estimator for $\mathbf{x}_i$' terminal node:

$$H(st|\boldsymbol{x}_i) = \widehat{H}_h(st). \quad (2)$$

Equation 2 describes the CHF from an individual tree. The ensemble CHF is computed by averaging over *ntree* trees. The bootstrap ensemble CHF for sample i is defined below (the definition of OOB ensemble CHF please refer to Ishwaran et al., 2008):

$$H_e(st|\boldsymbol{x}_i) = \frac{1}{ntree} \sum_{n=1}^{ntree} H_n(st|\boldsymbol{x}_i), \quad (3)$$

where $H_n(st|\boldsymbol{x})$ is the CHF for a tree grown from the n^{th} bootstrap sample.

The survival function is a probability density function that describes the survival probability at a given ST. In RSF, the ensemble survival function (S_e) could be derived from ensemble CHF (Mogensen et al., 2012):

$$S_e(st|\boldsymbol{x}_i) = \exp\left\{-\frac{1}{ntree} \sum_{n=1}^{ntree} H_n(st|\boldsymbol{x}_i)\right\}. \quad (4)$$

Here, the survival probability at a given ST is equal to the probability of exceeding a given ST or censored probability at a given ST. The probability of

exceeding a given ST ranges from 0 to 1, and when it is close to 1, the location has a high probability of being censored. Therefore, in this latter case, the actual ST has a high probability of being thicker than the censored ST.

Node splitting rule

The node splitting rule is another important parameter in RSF. There are several choices for splitting rules, including the log-rank splitting rule, conservation splitting rule, log-rank score rule, and fast approximation to the log-rank splitting. Here, the log-rank splitting rule is used as the default splitting rule, as suggested by Ishwaran et al. (2008). We define $st_1 < st_2 < \cdots < st_i$ as the ST intervals and $x_{i,j}$ and $a_{i,j}$ as the number of samples and number of actual ST samples at ST st_i in the sub-nodes j (1 or 2), respectively. Here, $x_i = x_{i,1} + x_{i,2}$ and $a_i = a_{i,1} + a_{i,2}$. The log-rank test for a split at the value n of the covariate c is defined as

$$L(c,n) = \frac{\sum_{i=1}^{I}(a_{i,1} - x_{i,1}\frac{a_i}{x_i})}{\sqrt{\sum_{i=1}^{I}\frac{x_{i,1}}{x_i}(1-\frac{x_{i,1}}{x_i})(\frac{x_i - a_i}{x_i - 1})a_i}}, \quad (5)$$

where the value $|L(c, n)|$ is the measure of node split, and $x_{i,1}$ and $a_{i,1}$ are the number of samples and number of actual ST samples, respectively, at ST st_i when c is less than n. The larger the $|L(c, n)|$ value, the larger the difference between two sub-nodes and a better split. The best split at each note is determined by searching the optimized covariate c^* and split value n^* to maximize the $|L(c, n)|$ value.

Prediction error

In survival analysis, Harrell's concordance index (Harrell Jr et al., 1982) is commonly used for estimating prediction error as it does not depend on choosing a fixed time for model evaluation and specifically accounts for censoring (May et al.,

2004). The concordance index (*C* index) is calculated by the following steps in ST modelling.

1) Generate all possible pairs of samples over the data.
2) Remove pairs whose lower ST is censored. Remove pairs *i* and *j* if $st_i = st_j$ unless at least one is an actual ST sample. The total number of permissible pairs is recorded as *Per*.
3) For each permissible pair where $st_i \neq st_j$: if the thinner ST has worse predicted outcome (higher cumulative hazard value), count 1; ii) otherwise, count 0.5. For each permissible pair where $st_i = st_j$ and both are actual ST samples: i) if predicted outcomes are equal, count 1; ii) otherwise, count 0.5. For each permissible pair where $st_i = st_j$ and not both, are actual ST samples: i) if the actual ST sample has a worse predicted outcome, count 1; ii) otherwise, count 0.5. The sum of all permissible pairs is recorded as *Con*.
4) The *C* index is defined by the ratio of *Con* to *Per*.

In RSF, the *C* index is computed via OOB data using the steps mentioned above, and it ranges between 0 and 1. The prediction error is calculated by the1-*C* index, so it is also between 0 and 1. A lower prediction error represents better model performance for the calibration model.

2.3.3. Assessing the main controlling factors for ST modelling

To assess the main controlling factors for ST in France, the variable importance of the ST predictors (i.e., covariates used) in the RSF model were evaluated. In RSF, the variable importance of a covariate *c* is calculated by dropping OOB samples down their in-bag survival tree. A sub-node is randomly assigned when encountering a split for *c*, and then an average of the CHF obtained from these

trees is calculated. The variable importance for *c* is calculated as the difference of prediction error between the new ensemble obtained using randomized *c* assignments and the original ensemble. A larger variable importance value indicates a higher contribution to the model for a covariate.

2.4. Soil thickness probability mapping and bootstrapping for determining prediction uncertainty

As introduced in Section 2.3.2, the RSF model outcome entails a function between the survival (censored) probability and ST for each prediction. In other words, the censored probability can be calculated over the full soil profile (0 to the maximum depth of actual ST samples) for any position in mainland France from RSF. As an example, the censored probabilities for the six *GlobalSoilMap* standard depths were extracted from the survival probability function (Fig. 3); those depths are 5, 15, 30, 60, 100, and 200 cm, which we refer to hereafter as ST5, ST15, ST30, ST60, ST100 and ST200, respectively. From this, we derived a probability map for each *GlobalSoilMap* standard depth in mainland France.

Bootstrapping was applied to determine the average and 90% Confidence Intervals (CIs) of the RSF model. Hence, we did not determine the 90% PIs as is recommended by the *GlobalSoilMap* specifications; instead we estimated the 90% CIs. This was deemed suitable, as we were not able to identify the random error in the RSF model. Consequently, the estimated 90% CIs would be narrower than 90% PIs. The bootstrap samples were drawn 50 times by repeated random sampling with replacement of the RMQS sites; the RMQS sites not used in each bootstrap sample were used to evaluate the model performance of each bootstrap RSF model (details in Section 2.5). Note that the bootstrap sample used here corresponds to the initial

301 data used in the RSF framework (Fig. 2), not the bootstrap sample used to generate
302 trees. Finally, using these bootstrap samples, 50 bootstrap RSF models were
303 generated, from which 50 probability functions between the censored probability and
304 ST could be exhaustively predicted for mainland France. After several iterative model
305 calibrations leading to the final prediction model, we choose 50 bootstrap models
306 because it is time-consuming to make predictions at a 90 m resolution for mainland
307 France (RSF produces a probability function rather than a value for each pixel, so it
308 takes 2 weeks for 50 bootstrap RSF models under parallel computing that make full
309 use of a computer with 8 cores and 32 GB of RAM). A robust estimate of the
310 probability of exceeding each standard *GlobalSoilMap* soil depth was determined by
311 averaging the bootstrap predictions. Their lower and upper 90% CIs were calculated
312 by the averaged bootstrap predictions minus and plus 1.645 times (Z score for 90%
313 CIs) the standard deviation of bootstrap predictions, respectively. Surface area
314 percentages of five probability intervals (0-0.2, 0.2-0.4, 0.4-0.6, 0.6-0.8, and 0.8-1)
315 were calculated from the averaged bootstrap predictions of probability maps at six
316 *GlobalSoilMap* standard depths. The mean probability was computed by averaging
317 all pixels of the probability map for each *GlobalSoilMap* standard depth.
318
319 2.5. Model performance
320 In addition to the CIs, the model performance of each *GlobalSoilMap* standard
321 depth was evaluated using the RMQS sites that were not used in the bootstrap
322 samples, which referred to an evaluation dataset from each bootstrap RSF model.
323 For a given *GlobalSoilMap* standard depth (st_s), the prediction performance was
324 evaluated based on the confusion matrix in which the misclassification rate was
325 calculated based on whether the data was censored or not. Hence, given a sample

with observed ST (st_o): 1) when $st_s \leqslant st_o$, if the probability exceeds 0.5, the sample is correctly predicted, otherwise, it is incorrectly predicted; and 2) when $st_s > st_o$, if the probability is less than 0.5, the sample is correctly predicted, otherwise, it is incorrectly predicted.

Subsequently, the confusion matrix was calculated as the mean counts of OOB samples with actual ST and censored ST separately from 50 bootstrap predictions.

All of the statistics and modelling were performed in R (R Core Team, 2016). R package *randomForestSRC* was used for RSF modelling (Ishwaran and Kogalur, 2017).

3. Results

3.1. Summary statistics of the ST dataset

Among 2108 RMQS sites, more than half were right censored for ST (Fig. 4). The actual ST ranged from 0 to 300 cm, with a mean value of 64 cm. The first quantile, median and third quantile were 39, 59, and 80 cm, respectively, indicating a large percentage of soils thinner than 60 cm. The censored ST ranged from 50 to 270 cm, with the mean ST (104 cm) being higher than the actual observed RMQS sites. For the censored RMQS sites, the first quantile, median, and third quantile were 75, 95, and 120 cm, respectively.

3.2. Model performance

The prediction error of the calibrated RSF models decreased from 0.27 to 0.15 as the number of trees increased up to 50 (Fig. 5). After 50 trees, the prediction error decreased slightly and became more stable as the number of trees increased (max.

300 trees). This indicated that 50 trees were sufficient for this study to produce a stable model while accelerating the prediction efficiency for big data.

The prediction performance differed when evaluated at the six *GlobalSoilMap* standard depths (Table 2). For the actual RMQS sites, the overall accuracy decreased from 0.989 to 0.546, when depth increased from ST5 to ST60. The overall accuracy then gradually increased up to 0.793 for ST200. The overall accuracy for censored RMQS sites were 1, 0.998, and 0.995, respectively, for SD5, SD15, and SD30, the accuracy then decreased to 0.825 for SD60 and subsequently dropped to 0.534 for ST100 and 0.563 for ST200.

3.3. Controlling factors of ST modelling

Parent material (PM) and climatic zones (TYPO) were the two most important variables affecting the ST probabilities in RSF models, based on the average bootstrap RSF (Fig. 6). The difference in prediction error between the new and the original ensembles was most affected by these two variables, despite the large 90% CIs. Roughness, precipitation, elevation, slope, gravimetry and Net Primary Production (NPP) also had large contributions in ST modelling. The remaining covariates contributed less to the RSF model and had smaller CIs.

3.4. ST probability maps and associated confidence intervals

Fig. 7 presents the ST probability maps of exceeding the six *GlobalSoilMap* standard depths and their 90% CIs for mainland France. Overall, the average probability of exceeding the *GlobalSoilMap* standard depths of 5, 15, 30, 60,100, and 200 cm were 0.99, 0.97, 0.88, 0.68, 0.51, and 0.42, respectively.

375 The probability of exceeding ST5 was close to 1 across the whole country,
376 except for eastern (the Alps) and southwestern France (the Pyrenees). The 90% CI
377 was very narrow (0.02 ± 0.06), indicating low model uncertainty and thus robust
378 estimates for the ST5 map.
379 A similar spatial distribution was observed when ST increased to ST15. The
380 low probability in southern France (the Massif Central) showed that this region had a
381 high probability of having STs less than 15 cm. The difference between the lower and
382 upper limits of the 90% CI was still low (0.05 ± 0.08), indicating a robust estimate.
383 Moreover, the surface area percentages for the five probability intervals were also
384 quite close to those of ST5 (Fig. 8).
385 When the ST depth criteria was further increased to ST30, in addition to
386 previously mentioned locations, low probabilities were found in eastern France (the
387 Jura Mountains, Fig. 7). Moreover, the CIs substantially increased (give numbers)
388 compared to ST5 and ST15. This indicates a larger prediction uncertainty and a
389 lower model robustness. In comparison with ST15, a slight increase (2%) was
390 observed for the surface area with probabilities between 0.4 and 0.6. The surface
391 area having a probability between 0.6 and 0.8 increased from 1 to 14%, while the
392 area with a probability between 0.8 and 1 decreased from 98 to 83% (Fig. 8).
393 Moving from the ST30 up to the ST200 thickness criteria, substantial changes
394 in spatial patterns and the probability of surpassing the ST criteria became apparent.
395 Most notable is how the surface area with probabilities between 0.8 and 1.0
396 continuously decreased, from 83% (ST30) to 2% (ST200). ST60 corresponded with a
397 probability of 27% and ST100 with a probability of 7% (Fig. 8).
398 For ST200, more than 50% of the territory of mainland France had a low
399 probability (<0.4) of exceeding ST by 2 m, while less than 17% of the areas had a

high probability (>0.6) of exceeding the ST by 2 m (Fig. 7). The areas with a high probability were mainly located in southwestern France (the Landes of Gascony), central France (Sologne), and northern France (thick loess deposits).

4. Discussion

Several ways to perform probability mapping have been proposed in the literature since the 1990s. For instance, Bell et al. (1994) applied discriminant analysis with a maximum-likelihood classification function to map the soil drainage probability in south-central Pennsylvania, USA. von Steiger et al. (1996) mapped the probability of exceeding the maximum tolerable heavy metal concentrations by Disjunctive Kriging in northeast Switzerland. Richer-de-Forges et al. (2017) used Logistic Regression Kriging in probability mapping of iron pan presence in sandy podzols in southwest France. The largest differences between the methods used in previous studies and RSF can be summarized in two aspects: 1) RSF is able to deal with right censored data while others are not, and 2) RSF can potentially produce probability estimates of any ST value, whereas other methods deal with presence/absence at a given threshold for the soil attributes of interest. Moreover, others used multiple sequential indicator simulations to model this type of distribution (e.g., Cattle et al., 2002). The survival analysis we used is a similar approach, except that it models the survival function rather than the empirical distribution function.

In the RMQS dataset, right censored ST observations entail more than half of the observations. Using them for ST modelling with traditional DSM approaches would result in highly underestimated ST estimates. Lacoste et al. (2016) proposed adding a fixed value of 30 cm to censored samples before modelling, which may help lower the underestimation but does not really solve the problem. Moreover, as actual

ST values of these censored sites remain unknown, adding a fixed value may even add more noise to the data, and thus enlarging the prediction uncertainty. As shown in Fig. 9, the probability of exceeding the observed ST for each censored RMQS site was mainly between 0.5 and 1, with a median value of 0.78. Thereafter, as outlined in the methodology Section 2.3.2, RSF makes use of the probability function derived from right censored information, thereby avoiding underestimating ST at these censored positions.

The mean probability of exceeding an ST of 100 cm across mainland France was 0.51 (Fig. 8), which means that all locations have a 50% possibility of being observed with an ST thicker than 100 cm. This result implies that the median ST in mainland France is approximately 100 cm, which is in line with previous work by Lacoste et al. (2016), showing that 48 and 54% of surface areas were below 100 cm when using Gradient Boosting Modelling and Cubist models, respectively.

The results showed that the prediction performance decreased from 0 to 60 cm and subsequently increased up to 200 cm for censored RMQS sites (Table 2), implying that the predicted probability of exceeding a given ST from the RSF model is more reliable for extreme values (i.e., a thin ST or thick ST). Indeed, due to the soil forming conditions in mainland France, except for steep slopes in mountainous areas, very thin soils are quite rare, and thus the probability of exceeding a very thin ST is high. Conversely, very thick soils are concentrated in (former) depositional areas (valleys, aeolian sand, or loess deposits) that can be easily mapped using some of the covariates (e.g., parent material and terrain parameters). For the censored RMQS sites, the overall accuracies for ST100 and ST200 were approximately 0.5, in which a large percentage of thin ST samples were misclassified as being thick. This can be explained by the fact that we used observed ST of censored RMQS sites in

450 calculating the confusion matrix. Consequently, we may overestimate the percentage
451 of misclassification mentioned before and thus underestimate the overall accuracies
452 of ST100 and ST200.

453 Parent material and climatic zones were the most important variables for
454 predicting ST in France using the bootstrapped RSF, but roughness, precipitation,
455 elevation, slope, gravimetry, and NPP also substantially contributed to the ST model.
456 These results are in line with previous findings reported by Lacoste et al. (2016).
457 Lacoste et al. (2016) stated that the most important covariates of ST modelling in
458 mainland France were soil properties, climate covariates and land use. Considering
459 the variable importance and the variables acting as controlling factors for ST, parent
460 material, climatic zones, precipitation, and gravimetry are direct drivers for the
461 weathering process. Roughness, elevation, slope, and NPP are more related to
462 sediment transport dynamics.

463 Future research should aim to derive an ST map using RSF, instead of the
464 currently presented ST probability map of exceeding a given depth. There are three
465 ways to determine the actual soil ST from the unique probability function produced by
466 RSF for each location of interest: 1) use the ST extracted from the median probability
467 in the predicted function; 2) use the ST extracted from a fixed probability, allowing the
468 classification of censored and actual ST at high accuracy among RSF calibration
469 datasets; 3) perform a derivative analysis on the probability curve. Moreover,it will be
470 interesting to combine RSF with geostatistical methods. For example, kriging of
471 residuals (Hengl et al., 2004) that are not captured by RSF and/or sampling
472 optimizing for future campaigns to reduce the prediction variance at locations where it
473 is highest. Alternatively, the presented probability maps can be used directly for
474 additional ST sampling campaigns, aimed at ST modelling in mainland France. For

example, the regions with a high probability (>0.8) of ST200 have a large chance of being censored. Integrating those high probability regions with parent material and climatic zones would yield an efficient and effective sampling design using conditioned Latin hypercube sampling (cLHS, Minasny and McBratney, 2006) to obtain more representative samples of all physiographic contexts. RSF is able to provide a probability at any depth and thus will be helpful for decision making in geotechnical engineering regarding, for example, laying out drains, pipes, and tubes (Zhang et al., 2005).

5. Conclusions

This study introduced the use of RSF in ST probability modelling to deal with right censored data for Digital Soil Mapping. RSF produced a probability function of ST for each soil sample included in the database. This function allowed the estimation of a probability of exceeding a given ST, indicating each soil location was right censored or not. Robust estimates were made by bootstrapping the RSF model to quantify an averaged bootstrap prediction and 90% CI for each *GlobalSoilMap* standard depth (5, 15, 30, 60, 100 and 200 cm) using the RSF survival probability functions. The model evaluation indicated an overall good performance (overall accuracy from 0.546 to 0.989) of RSF to predict the probability exceeding the six *GlobalSoilMap* standard depths. The RSF proved suitable for using right censored soil data for digital soil mapping, and thereby this work introduced a new approach capable of using both right censored and actual data for modelling ST accordingly.

Acknowledgement

The collection and handling of soil data was supported by the French Scientific Group of Interest on soils (GIS Sol), including the French Ministry of Ecology, the

French Ministry of Agriculture, the French Environment and Energy Management Agency (ADEME), the French Institute for Research and Development (IRD), the French Institute for National Geographic and Forest Information (IGN) and the National Institute for Agronomic Research (INRA). We thank all the people involved in sampling the sites and populating the database. We would also like to thank Quentin Styc and Philippe Lagacherie for sharing their ideas on dealing with right censored data. Songchao Chen received the support of the China Scholarship Council for three years' of Ph.D. study in INRA and Agrocampus Ouest (under grant agreement no. 201606320211).

References

Achache, J., Debeglia, N., Grandjean, G., Guillen, A., Le Bel, L., Ledru., P., Renaud, X., Autran,A., Bonijoly, D., Calcagno, P., Pluchery, E., Guennoc, P., Truffert, C., Rossi, P., Vairon, J.,Avouac, J.P., Poli, E., Senechal, G., Brun, J.P., Galdeano, A., Diament, M., Tarits, P., Mervier, J., Paul, A., Poupinet, G., Marquis, G., Bayer, R., Chautra, J.M., 1997.GEOFRANCE 3D: l'imagerie geologique et geophysique 3D du sous-sol de la France. Mémoires de la Société Géologique de France, 172, 53–71.

Andersen, P.K., Gill, R.D., 1982. Cox's regression model for counting processes: a large sample study. The Annals of Statistics 10(4), 1100–1120.

Arrouays, D., Grundy, M.G., Hartemink, A.E., Hempel, J.W., Heuvelink, G.B.M., Hong, S.Y., Lagacherie, P., Lelyk, G., McBratney, A.B., McKenzie, N.J., Mendonca-Santos, M.d.L., Minasny, B., Montanarella, L., Odeh, I.O.A., Sanchez, P.A., Thompson, J.A., Zhang, G.-L., 2014a. Chapter Three — GlobalSoilMap: Toward a Fine-Resolution Global Grid of Soil Properties. Adv. Agron. 125, 93–134.

525 Arrouays, D., McKenzie, N.J., Hempel, J., Richer de Forges, A.C., McBratney, A.,
526 2014b. GlobalSoilMap: Basis of the Global Spatial Soil Information System. 1st
527 ed. CRC Press Taylor & Francis Group.
528 Batjes, N.H., 1996. Total carbon and nitrogen in the soils of the world. Eur. J. Soil Sci.
529 47(2), 151–163.
530 Bell, J.C., Cunningham, R.L., Havens, M.W., 1994. Soil drainage class probability
531 mapping using a soil-landscape model. Soil Sci. Soc. Am. J. 58(2), 464–470.
532 Bonfatti, B.R., Hartemink, A.E., Vanwalleghem, T., Minasny, B., Giasson, E., 2018. A
533 mechanistic model to predict soil thickness in a valley area of Rio Grande do Sul,
534 Brazil. Geoderma 309, 17–31.
535 Bouma, J., 2018. The challenge of soil science meeting society's demands in a “post-
536 truth”,“fact free” world. Geoderma 310, 22-28.
537 Bourennane, H., King, D., Chery, P., Bruand, A., 1996. Improving the kriging of a soil
538 variable using slope gradient as external drift. Euro. J. Soil Sci. 47(4), 473–483.
539 Breiman, L., 2001. Random forests. Mach. Learn. 45(1), 5–32.
540 Cattle, J.A., McBratney, A., Minasny, B., 2002. Kriging method evaluation for
541 assessing the spatial distribution of urban soil lead contamination. J. Environ.
542 Qual. 31(5), 1576–1588.
543 Cerdan, O., Govers, G., Le Bissonnais, Y., Van Oost, K., Poesen, J., Saby, N., Gobin,
544 A., Vacca, A., Quinton, J., Auerswald, K., Klik, A., Kwaad, F.J.P.M., Raclot, D.,
545 Ionita, I., Rejman, J., Rousseva, S., Muxart, T., Roxo, M.J., Dostal, T., 2010.
546 Rates and spatial variations of soil erosion in Europe: A study based on erosion
547 plot data. Geomorphology 122, 167–177.
548 Chen, S., Arrouays, D., Angers, D.A., Chenu, C., Barré, P., Martin, M.P., Saby, N.P.
549 and Walter, C., 2019. National estimation of soil organic carbon storage potential

for arable soils: A data-driven approach coupled with carbon-landscape zones. Sci. Total Environ. 666, 355–367.

Chen, S., Martin, M.P., Saby, N.P., Walter, C., Angers, D.A., Arrouays, D., 2018. Fine resolution map of top-and subsoil carbon sequestration potential in France. Sci. Total Environ. 630, 389–400.

Clothier, B.E., Hall, A.J., Deurer, M., Green, S.R., Mackay, A.D., 2011. Soil ecosystem services: sustaining returns on investment into natural capital. In: Sauer, T.J., Norman, J.M., Sivakumar, M.V.K. (Eds.), Sustaining Soil Productivity in Response to Global Climate Change: Science, Policy, and Ethics. Wiley-Blackwell, Oxford, pp. 117–139.

De Oliveira, V., 2005. Bayesian inference and prediction of Gaussian random fields based on censored data. J. Comput. Graph. Stat. 14(1), 95–115.

Dietrich, W.E., Reiss, R., Hsu, M.L., Montgomery, D.R., 1995. A process - based model for colluvial soil depth and shallow landsliding using digital elevation data. Hydrol. Process. 9(3–4), 383–400.

Faroux, S., Tchuenté, A.K., Roujean, J.L., Masson, V., Martin, E., Le Moigne, P., 2013. ECOCLIMAP-II/Europe: A twofold database of ecosystems and surface parameters at 1 km resolution based on satellite information for use in land surface, meteorological and climate models. Geosci. Model Dev. 6(2), 563–582.

Feranec, J., Jaffrain, G., Soukup, T., Hazeu, G., 2010. Determining changes and flows in European landscapes 1990–2000 using Corine land cover data. Appl. Geogr. 30(1), 19–35.

Fridley, B. L., Dixon, P., 2007. Data augmentation for a Bayesian spatial model involving censored observations. Environmetrics 18(2), 107–123.

574 Groshans, G.R., Mikhailova, E.A., Post, C.J., Schlautman, M.A., 2018. Accounting for
575 soil inorganic carbon in the ecosystem services framework for United Nations
576 sustainable development goals. Geoderma 324, 37–46.
577 Harrell Jr, F.E., Califf, R.M., Pryor, D.B., Lee, K.L., Rosati, R.A., 1982. Evaluating the
578 yield of medical tests. Jama 247(18), 2543–2546.
579 Heimsath, A.M., Dietrich, W.E., Nishiizumi, K., Finkel, R.C., 1997. The soil production
580 function and landscape equilibrium. Nature 388, 358–361.
581 Heimsath, A.M., Dietrich, W.E., Nishiizumi, K., Finkel, R.C., 1999. Cosmogenic
582 nuclides, topography, and the spatial variation of soil depth. Geomorphology
583 27(1-2), 151–172.
584 Heimsath, A.M., Dietrich, W.E., Nishiizumi, K., Finkel, R.C., 2001. Stochastic
585 processes of soil production and transport: Erosion rates, topographic variation
586 and cosmogenic nuclides in the Oregon Coast Range. Earth Surf. Proc. Land.
587 26(5), 531–552.
588 Hengl, T., Heuvelink, G.B., Stein, A., 2004. A generic framework for spatial prediction
589 of soil variables based on regression-kriging. Geoderma 120(1–2), 75–93.
590 Hijmans, R.J., Cameron, S.E., Parra, J.L., Jones, P.G., Jarvis, A., 2005. Very high
591 resolution interpolated climate surfaces for global land areas. Int. J. Climatol. 25,
592 1965–1978.
593 Info Terre – Site cartographique de référence sur les géosciences, 2014. Indice de
594 développement et de persistance des réseaux (IDPR), edited, BRGM – Centre
595 scientifique et technique, Orléans, France.
596 Inglada, J., Vincent, A., Arias, M., Tardy, B., Morin, D., Rodes, I., 2017. Operational
597 high resolution land cover map production at the country scale using satellite
598 image time series. Remote Sens. 9(1), 95.

599 Inventaire Forestier National, 2006. BD Forêt® In: Service de l'inventaire forestier et
600 statistique - Institut national de l'information géographique et forestière (IGN)
601 (Ed.), Nogent-sur-Vernisson, 613 France.
602 Ishwaran H., Kogalur U.B., 2017. Random Forests for Survival, Regression, and
603 Classification (RF-SRC). R package version 2.5.1.
604 Ishwaran, H., Kogalur, U.B., Blackstone, E.H., Lauer, M.S., 2008. Random survival
605 forests. The Annals of Applied Statistics 2(3), 841–860.
606 IUSS Working Group, WRB, 2006. World reference base for soil resources. World
607 Soil Resources Report. 103.
608 Jarvis, A., Reuter, H.I., Nelson, A., Guevara, E., 2008. Hole-filled srtmfor the globe
609 version 4. available from the CGIAR-CSI SRTM 90m Database.
610 http://srtm.csi.cgiar.org.
611 Jenny, H., 1941. Factors of Soil Formation: A System of Quantitative Pedology.
612 McGrawHill, New York, pp.1–20.
613 Jolivet, C., Arrouays, D., Boulonne, L., Ratié, C., Saby, N., 2006. Le Réseau de
614 Mesures de la Qualité des Sols de France (RMQS). État d'avancement et
615 premiers résultats. Étude et Gestion Sols 13, 149–164.
616 Joly, D., Brossard, T., Cardot, H., Cavailhes, J., Hilal, M., Wavresky, P., 2010. Les
617 types de climats en France, une construction spatiale. Cybergeo: European
618 Journal of Geography.
619 Kaplan, E.L., Meier, P., 1958. Nonparametric estimation from incomplete
620 observations. J. Am. Stat. Assoc. 53(282), 457–481.
621 Keesstra, S.D., Bouma, J., Wallinga, J., Tittonell, P., Smith, P., Cerdà, A.,
622 Montanarella, L., Quinton, J.N., Pachepsky, Y., van der Putten, W.H., Bardgett,

623 R.D., 2016. The significance of soils and soil science towards realization of the
624 United Nations Sustainable Development Goals. Soil 2(2), 111–128.
625 Kempen, B., Brus, D.J., de Vries, F., 2015. Operationalizing digital soil mapping for
626 nationwide updating of the 1: 50,000 soil map of the Netherlands. Geoderma
627 241, 313–329.
628 King, D., Jones, R., Thomasson, A., 1995. European Land Information Systems for
629 Agro-Environmental Monitoring.
630 Knotters, M., Brus, D.J., Voshaar, J.O., 1995. A comparison of kriging, co-kriging and
631 kriging combined with regression for spatial interpolation of horizon depth with
632 censored observations. Geoderma 67(3–4), 227–246.
633 Kuriakose, S.L., Devkota, S., Rossiter, D.G., Jetten, V.G., 2009. Prediction of soil
634 depth using environmental variables in an anthropogenic landscape, a case
635 study in the Western Ghats of Kerala, India. Catena 79(1), 27–38.
636 Lacoste, M., Mulder, V.L., Richer-de-Forges, A.C., Martin, M.P., Arrouays, D., 2016.
637 Evaluating large-extent spatial modeling approaches: A case study for soil depth
638 for France. Geoderma Regional 7(2), 137–152.
639 Leenaars, J.G., Claessens, L., Heuvelink, G.B., Hengl, T., González, M.R., van
640 Bussel, L.G., Guilpart, N., Yang, H., Cassman, K.G., 2018. Mapping rootable
641 depth and root zone plant-available water holding capacity of the soil of sub-
642 Saharan Africa. Geoderma 324, 18–36.
643 Marx, A., Erhard, M., Thober, S., Kumar, R., Schäfer, D., Samaniego, L., Zink, M.,
644 2019. Climate Change as Driver for Ecosystem Services Risk and Opportunities.
645 In Atlas of Ecosystem Services. Springer, Cham, pp. 173–178.
646 May, M., Royston, P., Egger, M., Justice, A.C., Sterne, J.A., 2004. Development and
647 validation of a prognostic model for survival time data: application to prognosis of

HIV positive patients treated with antiretroviral therapy. Stat. Med. 23(15), 2375–2398.

McBratney, A.B., Santos, M.M., Minasny, B., 2003. On digital soil mapping. Geoderma 117(1–2), 3–52.

Meyer, M.D., North, M.P., Gray, A.N., Zald, H.S., 2007. Influence of soil thickness on stand characteristics in a Sierra Nevada mixed-conifer forest. Plant Soil 294(1–2), 113–123.

Millennium Ecosystems Assessment. (2005). Ecosystems and human well-being: policy responses. Island Press, Washington, DC.

Minasny, B., McBratney, A.B., 1999. A rudimentary mechanistic model for soil production and landscape development. Geoderma 90(1–2), 3–21.

Minasny, B., McBratney, A. B., 2006. A conditioned Latin hypercube method for sampling in the presence of ancillary information. Comput. Geosci. 32(9), 1378–1388.

Mogensen, U.B., Ishwaran, H., Gerds, T.A., 2012. Evaluating random forests for survival analysis using prediction error curves. J. Stat. Softw. 50(11), 1–23.

Moore, I.D., Gessler, P.E., Nielsen, G.A., Peterson, G.A., 1993. Soil attribute prediction using terrain analysis. Soil Sci. Soc. Am. J. 57(2), 443–452.

Mulder, V.L., Lacoste, M., Richer-de-Forges, A.C., Arrouays, D., 2016a. GlobalSoilMap France: High-resolution spatial modelling the soils of France up to two meter depth. Sci. Total Environ. 573, 1352–1369.

Mulder, V.L., Lacoste, M., Richer-de-Forges, A.C., Martin, M.P., Arrouays, D., 2016b. National versus global modelling the 3D distribution of soil organic carbon in mainland France. Geoderma 263, 16–34.

672 NASA LD, 2001. NASA Land Processes Distributed Active Archive Center (LP DAAC)
673 USGS/Earth Resources Observation and Science (EROS) Center.
674 Odeh, I.O.A., Chittleborough, D.J., McBratney, A.B., 1991. Elucidation of soil-
675 landform interrelationships by canonical ordination analysis. Geoderma 49(1–2),
676 1–32.
677 Odeh, I.O., McBratney, A.B., Chittleborough, D.J., 1995. Further results on prediction
678 of soil properties from terrain attributes: heterotopic cokriging and regression-
679 kriging. Geoderma 67(3–4), 215–226.
680 Orton, T. G., Rawlins, B. G., Lark, R. M., 2009. Using measurements close to a
681 detection limit in a geostatistical case study to predict selenium concentration in
682 topsoil. Geoderma 152(3–4), 269–282.
683 Orton, T.G., Saby, N., Arrouays, D., Jolivet, C.C., Villanneau, E.J., Paroissien, J.B.,
684 Marchant, B.P., Caria, G., Barriuso, E., Bispo, A., Briand, O., 2012. Analyzing
685 the spatial distribution of PCB concentrations in soils Using below–quantification
686 limit data. J. Environ. Qual. 41(6), 1893–1905.
687 Pelletier, J.D., Rasmussen, C., 2009. Geomorphically based predictive mapping of
688 soil thickness in upland watersheds. Water Resour. Res. 45(9), 417.
689 Penížek, V., Borůvka, L., 2006. Soil depth prediction supported by primary terrain
690 attributes: a comparison of methods. Plant Soil Environ. 52(9), 424–430.
691 Rabot, E., Wiesmeier, M., Schlüter, S., Vogel, H.J., 2018. Soil structure as an
692 indicator of soil functions: a review. Geoderma 314, 122–137.
693 R Core Team. R: A Language and Environment for Statistical Computing. R
694 Foundation for Statistical Computing, Vienna, Austria (2016), pp. 1.

695 Richer-de-Forges, A.C., Saby, N.P., Mulder, V.L., Laroche, B., Arrouays, D., 2017.
696 Probability mapping of iron pan presence in sandy podzols in South-West
697 France, using digital soil mapping. Geoderma Regional 9, 39–46.
698 Román Dobarco, M., Bourennane, H., Arrouays, D., Saby, N.P.A., Cousin, I., Martin,
699 M.P., 2019. Uncertainty assessment of *GlobalSoilMap* soil available water
700 capacity products: a French case study. Geoderma 344, 14–30.
701 Román, J.R., Roncero‐Ramos, B., Chamizo, S., Rodríguez‐Caballero, E. and
702 Cantón, Y., 2018. Restoring soil functions by means of cyanobacteria inoculation:
703 importance of soil conditions and species selection. Land Degrad. Dev. 29(9),
704 3184–3193.
705 Sanchez, P.A., Ahamed, S., Carré, F., Hartemink, A.E., Hempel, J., Huising, J.,
706 Lagacherie, P., McBratney, A.B., McKenzie, N.J., Mendonça-Santos, M.dL.,
707 Minasny, B., Montanarella, L., Okoth, P., Palm, C.A., Sachs, J.D., Shepherd,
708 K.D., Vågen, T.G., Vanlauwe, B., Walsh, M.G., Winowieki, L.A., Zhang, G.L.,
709 2009. Digital soil map of the world. Science 325 (5941), 680–681.
710 Shangguan, W., Hengl, T., Mendes de Jesus, J., Yuan, H., Dai, Y., 2017. Mapping
711 the global depth to bedrock for land surface modeling. J. Adv. in Model Earth Sy.
712 9(1), 65–88.
713 Soil Survey Division Staff, 1993. Soil survey manual. Soil conservation service U.S.
714 Department of Agriculture Handbook, pp.18.
715 Styc, Q., Lagacherie, P., 2016. Predicting soil depth using a survival analysis model.
716 Oral presentation at the 7th Global Workshop on Digital Soil Mapping, Aarhus,
717 Denmark, 27 June to 1 July.

718 Tesfa, T.K., Tarboton, D.G., Chandler, D.G., McNamara, J.P., 2009. Modeling soil
719 depth from topographic and land cover attributes. Water Resour. Res. 45(10),
720 438.
721 Vanwalleghem, T., Poesen, J., McBratney, A., Deckers, J., 2010. Spatial variability of
722 soil horizon depth in natural loess-derived soils. Geoderma 157(1–2), 37–45.
723 Vaysse, K., Lagacherie, P., 2015. Evaluating digital soil mapping approaches for
724 mapping GlobalSoilMap soil properties from legacy data in Languedoc-
725 Roussillon (France). Geoderma Regional 4, 20–30.
726 Vogel, H.J., Bartke, S., Daedlow, K., Helming, K., Kögel-Knabner, I., Lang, B., Rabot,
727 E., Russell, D., Stößel, B., Weller, U., Wiesmeier, M., 2018. A systemic approach
728 for modeling soil functions. Soil 4(1), 83–92.
729 Von Steiger, B., Webster, R., Schulin, R., Lehmann, R., 1996. Mapping heavy metals
730 in polluted soil by disjunctive kriging. Environmental Pollution 94(2), 205–215.
731 Wang, J., Endreny, T.A., Hassett, J.M., 2006. Power function decay of hydraulic
732 conductivity for a TOPMODEL ‐ based infiltration routine. Hydrol. Process.
733 20(18), 3825–3834.
734 Zhang, T., Frauenfeld, O.W., Serreze, M.C., Etringer, A., Oelke, C., McCreight, J.,
735 Barry, R.G., Gilichinsky, D., Yang, D., Ye, H., Ling, F., 2005. Spatial and
736 temporal variability in active layer thickness over the Russian Arctic drainage
737 basin. Journal of Geophysical Research: Atmospheres 110, D16101.
738 Zhu, A.X., Hudson, B., Burt, J., Lubich, K., Simonson, D., 2001. Soil mapping using
739 GIS, expert knowledge, and fuzzy logic. Soil Sci. Soc. Am. J. 65(5), 1463–1472.
740

Figures

Fig. 1 Locations of RMQS sites with actual (dotted) and censored (star) ST values. For each site, ST is classified based on the *GlobalSoilMap* standard depths. Corine Land Cover map of 2006 of mainland France (right) with the administrative regions (black italics) and natural geographic regions (blue italics).

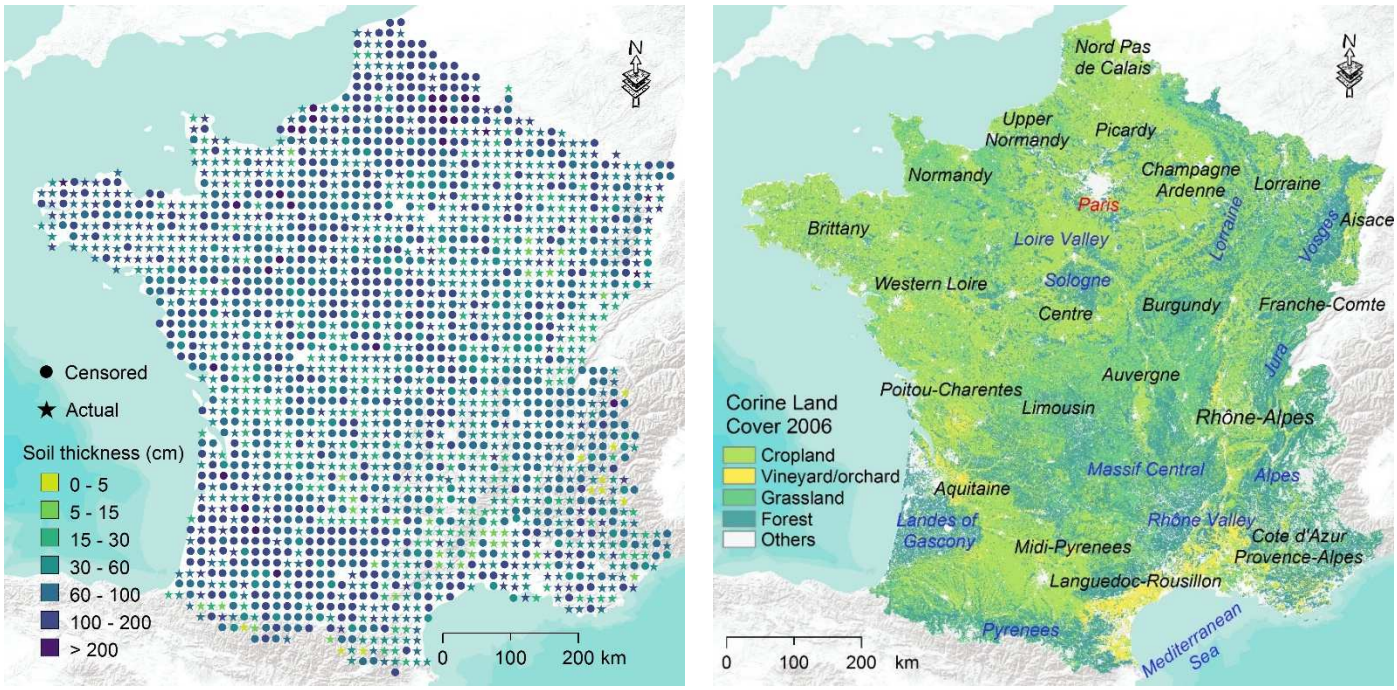

747 Fig. 2 Random survival forest workflow.

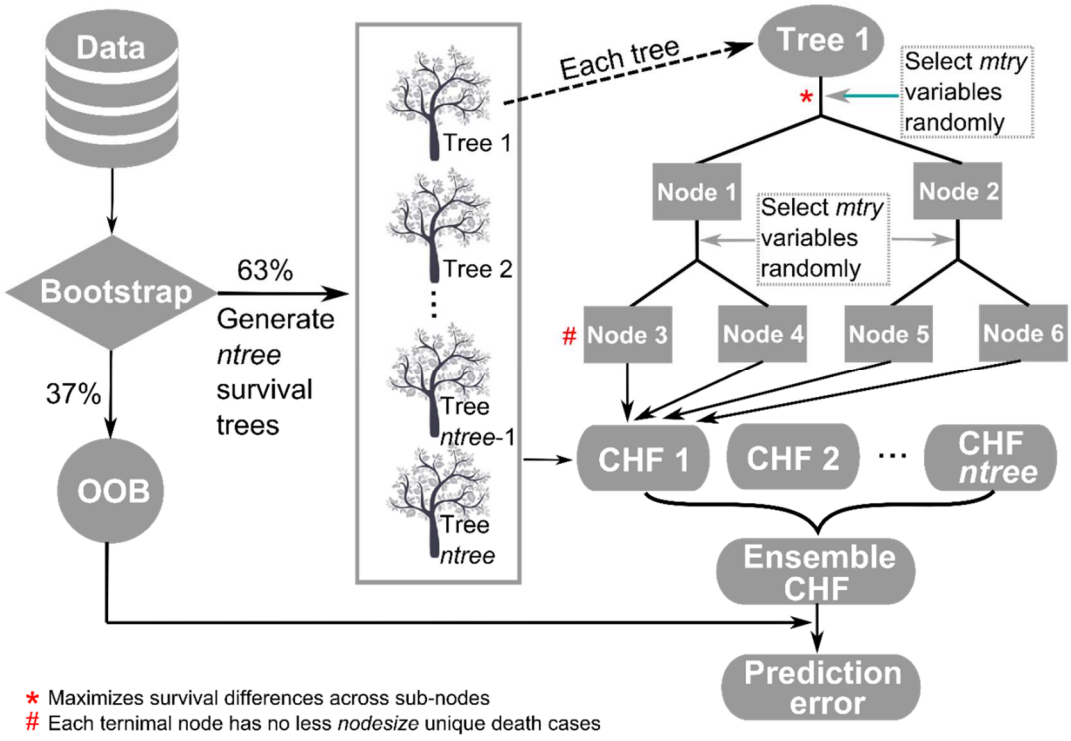

748

749

Fig. 3 Survival probability curve (blue solid line) for one location predicted by RSF. The orange dashed vertical lines indicate the six *GlobalSoilMap* standard depths, and the orange dashed horizontal lines indicate their corresponding censored probabilities that are derived from the survival probability curve.

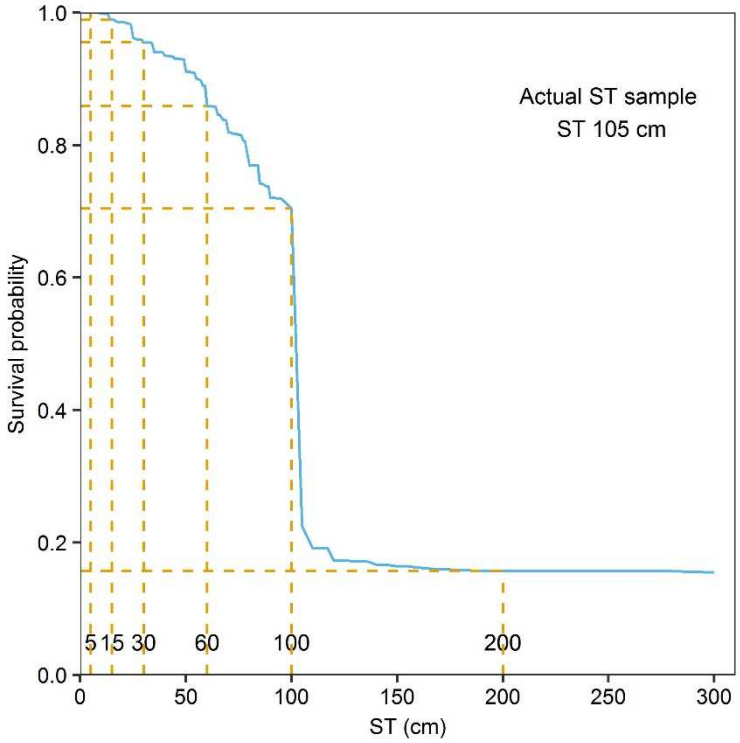

Fig. 4 Density distribution of STs for actual and censored RMQS sites. Counts of actual and censored samples within *GlobalSoilMap* depth intervals are provided.

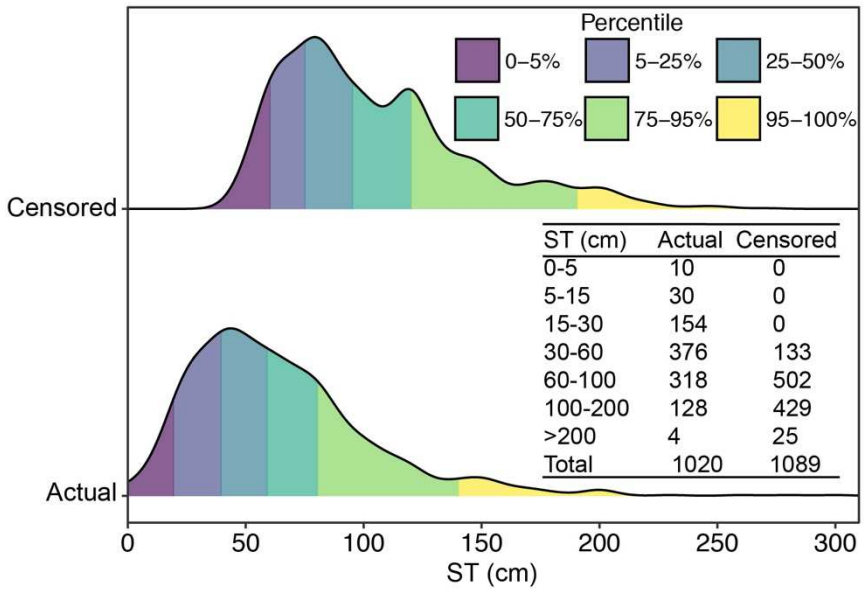

ST (cm)	Actual	Censored
0-5	10	0
5-15	30	0
15-30	154	0
30-60	376	133
60-100	318	502
100-200	128	429
>200	4	25
Total	1020	1089

760 Fig. 5 Mean and 90% confidence intervals of the prediction error, given different
761 numbers of trees from 50 bootstrapping random survival forests.

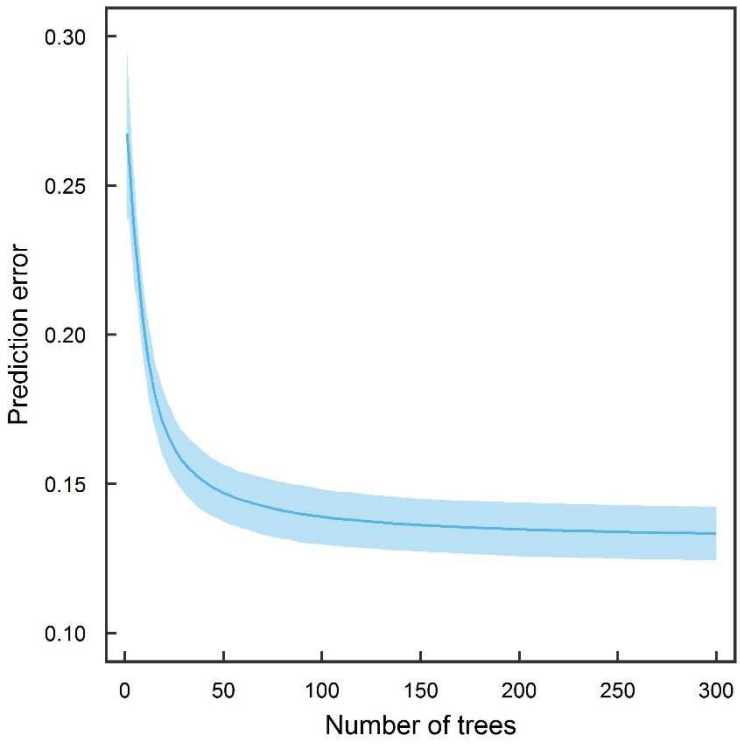

762

763 Fig. 6 Mean and 90% confidence intervals of variable importance from 50
764 bootstrapping random survival forests.

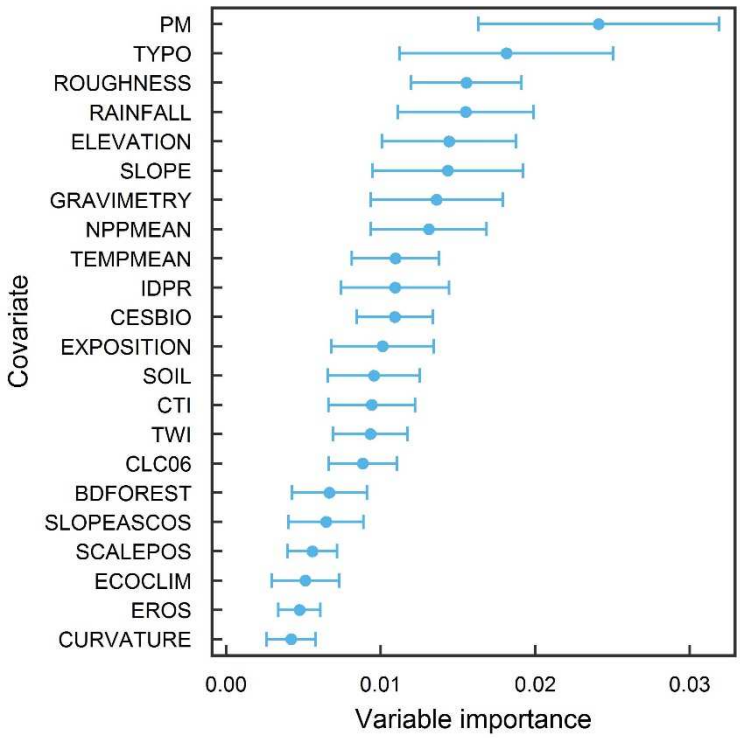

765

766 Fig. 7 Probability maps of exceeding the six *GlobalSoilMap* standard depths (middle)
767 and their associated 90% confidence intervals (left and right).

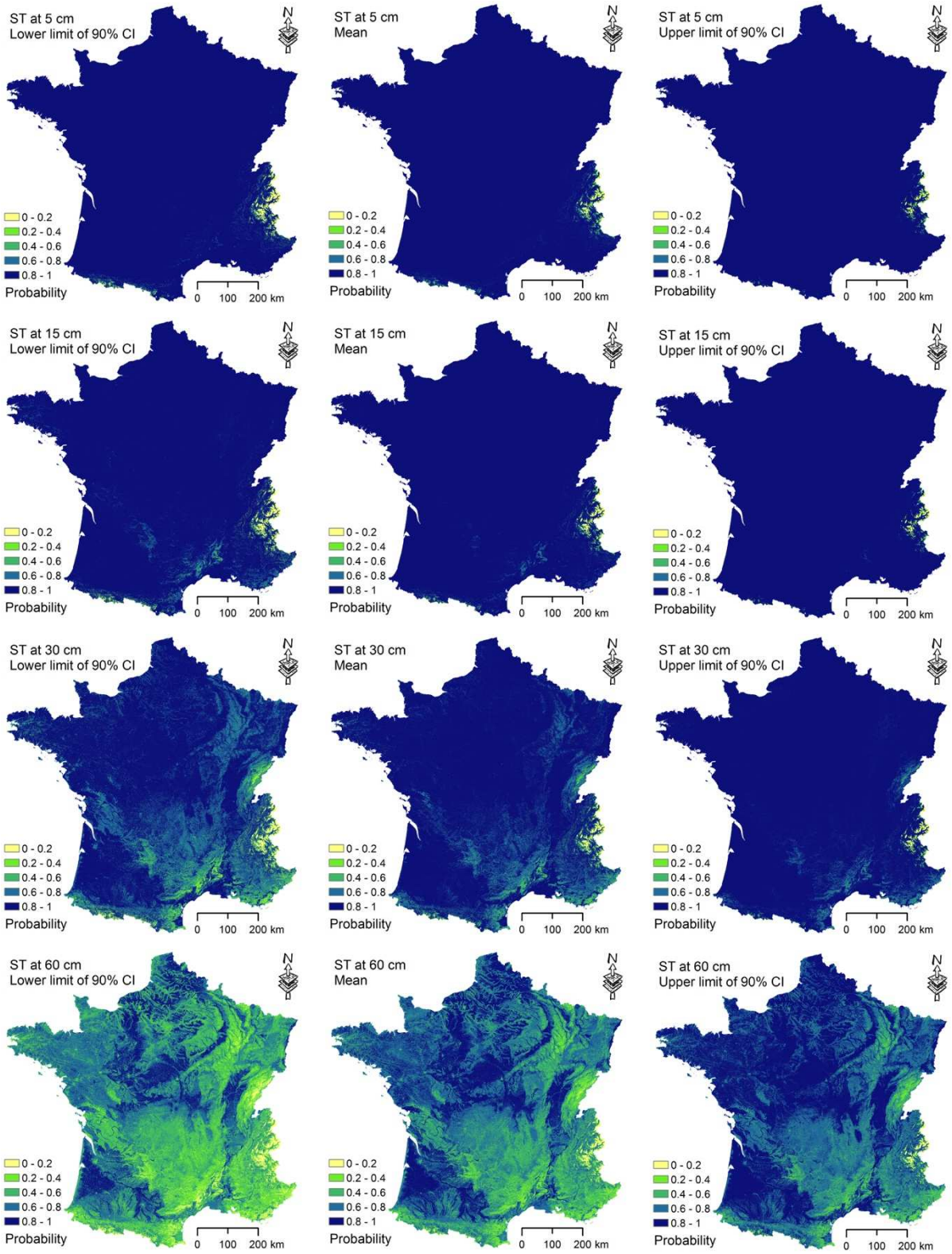

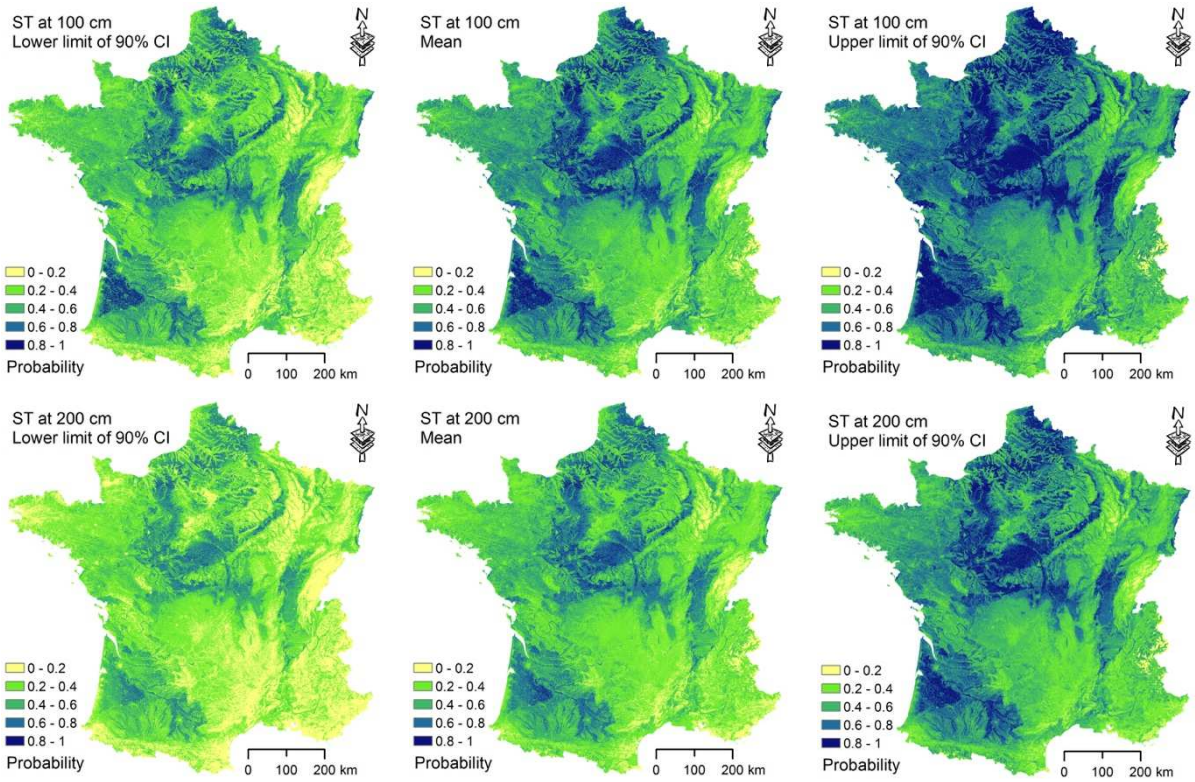
ST at 100 cm
Lower limit of 90% CI
ST at 100 cm
Mean
ST at 100 cm
Upper limit of 90% CI
ST at 200 cm
Lower limit of 90% CI
ST at 200 cm
Mean
ST at 200 cm
Upper limit of 90% CI
N
0 - 0.2
0.2 - 0.4
0.4 - 0.6
0.6 - 0.8
0.8 - 1
Probability
0 100 200 km

768 Fig. 8 Surface area percentage of the probability of exceeding the ST of each
769 *GlobalSoilMap* standard depths. The mean probability is calculated by averaging all
770 the pixels in the probability map for each *GlobalSoilMap* standard depth.

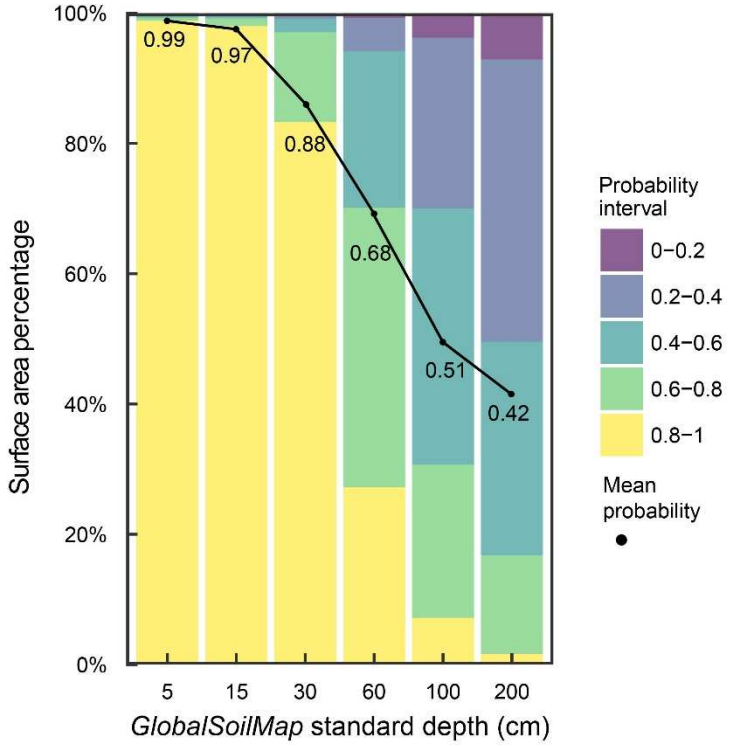

771

772 Fig. 9 Histogram with the probability of exceeding the observed ST for each censored
773 RMQS site.

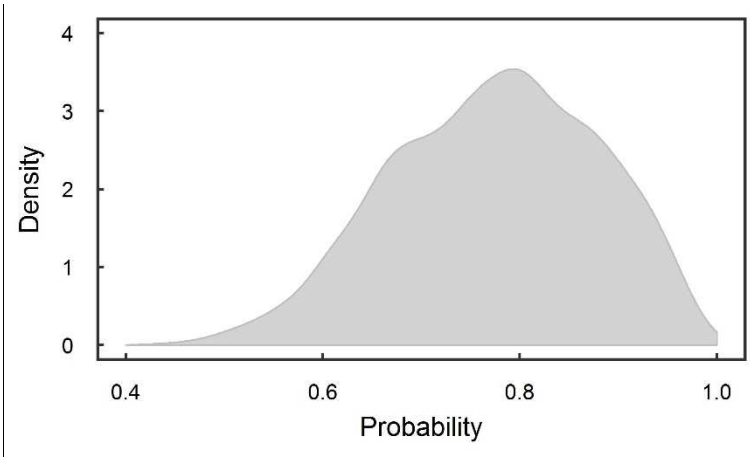

774
775

Tables

Table 1 Exhaustive covariates used for ST modelling (after Mulder et al., 2016b)

Variable	Abbreviation	Scale/resolution	Soil forming factor	Reference
Elevation	ELEVATION	90 m	Relief	Jarvis et al. (2008)
Compound topographic index	CTI	90 m	Relief	Jarvis et al. (2008)
Curvature	CURVATURE	90 m	Relief	Jarvis et al. (2008)
Exposition	EXPOSITION	90 m	Relief	Jarvis et al. (2008)
Roughness	ROUGHNESS	90 m	Relief	Jarvis et al. (2008)
Slope	SLOPE	90 m	Relief	Jarvis et al. (2008)
Slope cosines	SLOPECOS	90 m	Relief	Jarvis et al. (2008)
Slope position	SLOPEPOS	90 m	Relief	Jarvis et al. (2008)
Topographic wetness index	TWI	90 m	Relief	Jarvis et al. (2008)
Gravimetric data (Bouguer anomaly)	GREVIMETRY	4 km	Relief	Achache et al. (1997)
Soil type[a]	SOIL	1:1000000	Soil	IUSS Working Group WRB (2006)
Erosion rates	EROS	1:1000000	Soil	Cerdan et al. (2010)
Rate of river network development and persistence	IDPR	1:50000	Soil and parent material	Info Terre – Site cartographique de référence sur les géosciences (2014)
Parent material	PM	1:1000000	Parent material	King et al. (1995)
Mean annual net primary production	NPPMEAN	1 km	Organisms	NASA LD (2001)
Forest type	BDFOREST	Min area 2.25 ha	Organisms	Inventaire Forestier National (2006)
Land cover from Sentinel-2	LCS	10 m	Organisms	Inglada et al. (2017)
Corine land cover 2006	CLC06	250 m	Organisms	Feranec et al. (2010)
ECOCLIMAP land use	ECOCLIM	1 km	Organisms	Faroux et al. (2013)
Climatic zones	TYPO	1 km	Climate	Joly et al. (2010)
Mean annual precipitation	RAINFALL	1 km	Climate	Hijmans et al. (2005)
Mean annual temperature	TEMPMEAN	1 km	Climate	Hijmans et al. (2005)

[a] Soil type defined by World Reference Base (WRB)

779 Table 2 Model performance of actual and censored RMQS sites per each
780 *GlobalSoilMap* standard depth, based on out of bag samples. The count of correctly
781 classified sites is marked **bold**, and the overall accuracy is marked *italic underlined*.

ST (cm)		Actual RMQS sites			Censored RMQS sites		
	Predicted / Observed	Thin	Thick	Accuracy	Thin	Thick	Accuracy
5	Thin	**2**	2	0.500	**0**	0	1
	Thick	0	**367**	1	0	**400**	1
	Reliability	1	0.995	*0.989*	*n.a.*	1	*1*
15	Thin	**2**	12	0.143	**0**	0	*n.a.*
	Thick	0	**356**	1	1	**399**	1
	Reliability	1	0.967	*0.962*	0	1	*0.998*
30	Thin	**5**	65	0.063	**0**	0	*n.a.*
	Thick	1	**300**	0.997	2	**398**	1
	Reliability	0.833	0.843	*0.822*	0	1	*0.995*
60	Thin	**58**	150	0.279	**7**	43	0.140
	Thick	18	**144**	0.889	27	**323**	0.923
	Reliability	0.763	0.490	*0.546*	0.205	0.883	*0.825*
100	Thin	**203**	120	0.628	**97**	138	0.413
	Thick	19	**28**	0.596	49	**117**	0.705
	Reliability	0.914	0.189	*0.624*	0.664	0.459	*0.534*
200	Thin	**294**	76	0.795	**219**	172	0.560
	Thick	1	**1**	0.500	3	**6**	0.667
	Reliability	0.997	0.013	*0.793*	0.986	0.034	*0.563*

782 *n.a.* Not available.